NJC

Biomimetic Synthesis of Novel Calcium Carbonate Heterogeneous Dendrites

Journal:	*New Journal of Chemistry*
Manuscript ID:	NJ-ART-01-2015-000219.R1
Article Type:	Paper
Date Submitted by the Author:	23-Apr-2015
Complete List of Authors:	Ma, Li; Anhui Province Key Laboratory of Metallurgical Emission Reduction & Resources Recycling, Anhui University of Technology Zhu, Jianhua; Anhui Province Key Laboratory of Metallurgical Emission Reduction &Resources Recycling, Anhui University of Technology Cui, Mingfang; Anhui Province Key Laboratory of Metallurgical Emission Reduction & Resources Recycling, Anhui University of Technology Huang, Lei; Anhui Province Key Laboratory of Metallurgical Emission Reduction & Resources Recycling, Anhui University of Technology Su, Yiping; Anhui Province Key Laboratory of Metallurgical Emission Reduction & Resources Recycling, Anhui University of Technology

SCHOLARONE™
Manuscripts

Journal Name

ARTICLE

Biomimetic Synthesis of Novel Calcium Carbonate Heterogeneous Dendrites†

Li Ma, Jianhua Zhu[*], Mingfang Cui, Lei Huang, Yiping Su

Calcium carbonate dendrites with novel leaf- and snowflake-like morphology were synthesized with the combination of two different functional additives. They show fascinating heterogeneous domains made up of internal calcite scaffolding, aragonite shell and external amorphous calcium carbonate coating. They were formed in a gel-like solution composed of amorphous or liquid like mineral precursor. The developing dendrites arose from the correlation of solutes diffusion and driving force of crystallization. And their heterogeneous microstructures were determined by balance between thermodynamic and kinetic reaction. Our research provided a novel procedure towards the formation of heterogeneous inorganic superstructures with the synergistic effect of two different additives.

Introduction

Chemists have showed strong interest in synthesizing materials with exquisite morphology, selective polymorphs and amazing structures resembling those biominerals.[1] Their inspiration usually arose from key tenets in the biological systems. Investigation of the biogenic materials shows that their growth involves association with various insoluble organic matrices and soluble inorganic additives in localized environments,[2, 3] where a time-dependent interplay of different components results in sophisticated control over structure and properties.

Inspired by the natural strategy, scientists have applied various additives, such as low-mass molecules,[4] polyelectrolyte,[5] double hydrophilic block copolymers (DHBCs),[6] biomacromolecules,[7] organic matrices[8] and gel frameworks,[9] to operate the crystallization process. Following these synthetic approaches, a variety of morphologies have been produced, such as fibers,[10] helices,[11] plates,[12] and other complex microstructure.[13] Previous studies mainly focus on application of a single additive for crystallization control, whereas investigation on the cooperative mechanisms of two or more additives is still a challenge because of the complexity and difficulties in understanding the synergetic effect.[14]

In this research, we paid special attention to dendrite-shaped materials, which were frequently produced under a far non-equilibrium condition. They have special significance in understanding the growth behavior of branched fractal patterns and potential technological applications due to their dimensions and high surface area.[15] However, previous efforts were concentrated on the dendrites of noble metals and metal chalcogenide[16] synthesized by means of hydro/solvothermal[17] and electrochemical deposition.[18] However, limited knowledge was reported on formation mechanism of dendritic biomaterials formed in mild reaction environments.[19]

Herein, we report a biomimetic mineralization approach to synthesize calcium carbonate dendrites in the presence of two functional additives. The spontaneously formed gel-like solution would result into a far non-equilibrium reaction-diffusion field, which was favorable to the growth of dendrites. Thus, $CaCO_3$ heterogeneous dendrites of calcite and aragonite were synthesized within one system without any other ions (Mg^{2+}).[20] Further, by identifying physico-chemical changes in the mineral solution, we gained insight into their possible formation mechanisms. The ability to prepare such heterogeneous $CaCO_3$ dendrites opened the door to synthesize complex functional materials using two different synergetic additives.

Experimental

Materials and Preparation

Bovine serum albumin (BSA) (Part V) is of biotechnology grade. Others (calcium chloride and ammonium bicarbonate) are of analytical grade. All regents were purchased from Shanghai Chemical Reagent Company and used without further purification. Poly(sodium-p-styrenesulfonate) (PSS) ($Mw \approx 70000$ g mol^{-1}) was bought from Aldrich. All glassware was used after intensive cleaning with sulphuric-peroxide mixture (H_2SO_4: H_2O_2 = 4:1) and thorough rinsing with de-ionized water.

Mineralization

In a typical synthesis process, BSA and PSS were dissolved in 10 mL aqueous $CaCl_2$ solution (1M) under magnetic stirring, which was freshly prepared in boiled doubly distilled water and bubbled with N_2 for 2 h before use. It was then transferred into a glass bottle with small pieces of glass substrates at the bottom. Then they were covered with Parafilm with three needle holes, and placed in a desiccator at different temperature (10 or 25 ± 1°C). Finally, three glass bottles (10 mL) with crushed ammonium carbonate were covered with Parafilm with three needle holes were placed at the

bottom of the desiccator as the source of CO_2. After different
70 periods of reaction time, the Parafilm was removed. And small
pieces of glass substrates with precipitate were taken out from the
bottles to stop reaction. They were rinsed with distilled water and
ethanol and allowed to dry at room temperature. Early mineral
precursor was centrifuged at 10000 RPM from the solution, and
75 rinsed repeatedly with acetone. The solid was then transferred into
a vacuum drying oven for 6-8 h to complete drying of the samples.

Characterization

The phase of as-prepared products was characterized by X-ray
diffraction (XRD) pattern, which was recorded on a Germany D8
80 Advance diffraction system using a CuKα source (λ = 1.54178 Å)
at a scanning rate of 6 °/min. The scanning electron microscopy
(SEM) measurements were performed on a JEOL JSM-6700F field
emission scanning electron microscope (FE-SEM). Transmission
electron microscopy (TEM), high-resolution transmission electron
85 microscope (HRTEM) and selected area electron diffraction
patterns (SAED) were taken on a JEOL JEM 2011 microscope at
200 kV. Optical images were taken on the Leica microscope (DM
6000, German). Fourier transform infrared (FTIR) spectra were
obtained on a Nicolet 6700 FT-IR spectrometer from 400 to 4000
90 cm^{-1} at room temperature. Simultaneously thermogravimetric
analysis (TG) and differential scanning calorimetry (DSC) were
measured during the programmed heating (25-900°C at 10K/min)
using Netzsch STA 449 F3 (German) Jupiter instrument under a N_2
atmosphere. The size distribution was measured by a dynamic light
95 scattering (Dynapro-MS800 ATC, England). Ion selected
electrodes (ISE) were used to measure pH values and free calcium
concentration simultaneously (Mettler Toledo, Switzerland). The
ion chromatography (ICS-3000, Dionex Corporation, USA) was
performed using KOH as an eluent at pH 12, such that inorganic
100 carbon species are purely in the form of carbonate (CO_3^{2-}). Detailed
calculation about carbonate ion concentrations and saturation (S)
were provided in the supporting information. Polymer
concentrations were detected by high performance liquid
chromatography (HPLC) (Agilent 1260, German).

105 ## Results and Discussion

Heterostructured CaCO₃ dendrites
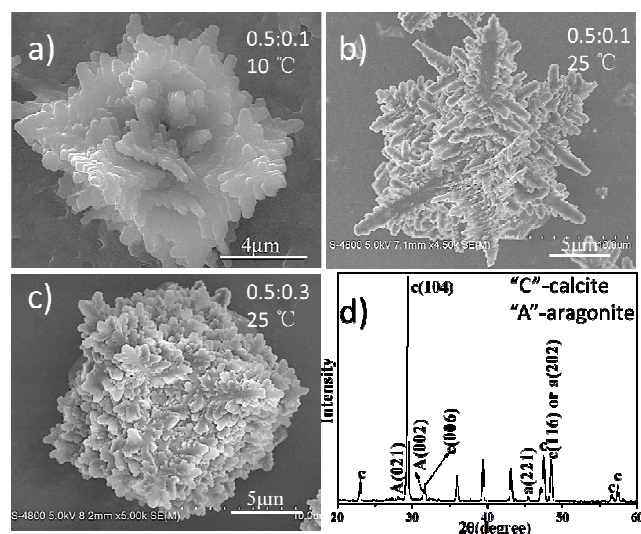
Fig. 1 SEM images of CaCO₃ dendrites obtained at different condition (a-c).
XRD pattern of carbonate samples (d). (Unit: g/L)

110 Fascinating CaCO₃ dendrites (Fig. 1a-c) were generated via a gas
diffusion procedure in the presence of BSA and PSS. They have a

mean size of 15~25 μm and display multilayered branches like
spring blossoms, trees or snowflakes. Fig. 1b presents the typical
dendrites that have three longer trunks and many branches
115 regularly arranged on their lateral surfaces. Magnified images
imply that branches may be original from the smaller nanorods
(Fig. S1, ESI†). The branch length becomes slightly smaller at
positions along the trunk that are further away from the center. At a
lower temperature of 10°C, nanobranches grow into leaf-like
120 structures with smooth surface (Fig. 1a), and multilevel three-fold
symmetrical snowflakes dendrites were synthesized with a higher
PSS concentration (Fig. 1c). Interestingly, XRD pattern indicates
that two polymorphs of calcite and aragonite are present in the
samples after 8 days (Fig. 1d). FT-IR spectrum further confirms the
125 coexistence of two crystal phases (Fig. S2, ESI†). The
characteristic vibrational bands of 712 and 875 cm^{-1} are clearly
indicative of calcite crystals. And the band at 849 cm^{-1} is relative to
aragonite phases. We examine many SEM images and find that
dendrites are the only crystals obtained in our experiments (Fig. S3,
130 ESI†). It is reasonable to infer that the synthesized dendrites are
heterostructures composed of calcite and aragonite. More detailed
data from TEM, HRTEM and SAED analysis will be provided to
prove above assumption.
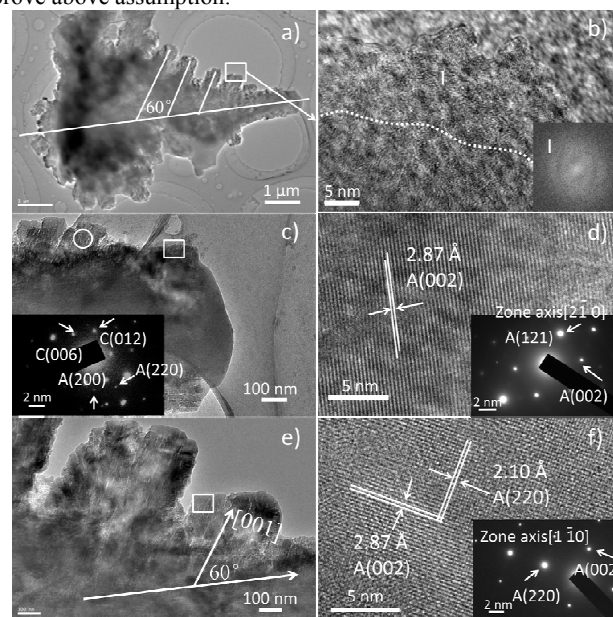
135 **Fig. 2** Left shows a typical dendrite TEM images. Right and inserts show
corresponding HRTEM images, FFT or SAED pattern.

Fig. 2a shows the typical TEM image of a small dendrite which
is composed of small branches and one main trunk. Small branches
parallel to each other form an angle about 60° with the main trunk
140 (Fig. 2c and 2e). HRTEM image reveals that most branches are
sheathed by an ACC layer about 20 nm (region I in Fig. 2b).
Corresponding FFT pattern corroborates that the external surface is
still amorphous (inset in Fig. 2b). Interestingly, under the intense
electron beam of the microscope, the thin layer transforms rapidly
145 into aragonite in one minute (Fig. S4, ESI†), which is similar to
some biogenic samples.[21] The ACC layer may work as a protective
coating,[22] restraining aragonite against transformation or re-
crystallization in the mineral solution.

HRTEM image of the trunk reveals the lattice fringes of
150 aragonite (002) planes (d = 2.87 Å), which is further validated by
SAED pattern (Fig. 2d and inset). It grows along the [001]
directions. HRTEM image of the small branches shows a typical
orthogonal matrix with the lattice spacings of 2.87 Å and 2.10 Å
(Fig. 2f), which can be well indexed to the (002) and (220) planes

of aragonite, respectively. The relative SAED pattern (inset in Fig. 2f) further proves that they are aragonite crystals along the [001] direction (Fig. 2e). Specially, ED analysis in the region close to the trunk (Fig. 2c) displays patterns of calcite and aragonite phases (inset in Fig. 2c). Unfortunately, the HRTEM images are not easy to obtain. Previous reports indicated that heterostructured minerals of calcite to aragonite could form via various pathways, such as lattice dislocation [23] and amorphous coating. [24] We will further discuss the transformation process in following section.

To investigate the effect of different additives on the final product, their concentrations were varied. Experiments indicate that the concentration of additives and their ratio have a distinct influence on the polymorphs of dendrite crystals. At a fixed BSA concentration (0.5 g/L), PSS needs to keep below 0.3 g/L at a constant BSA concentration (0.5 g/L) to obtain the heterogeneous microstructures (Fig. S10-11, SEI†). Higher PSS concentrations (>0.3 g/L) will result into the formation of pure calcite crystals, suggesting that aragonite phase can not form from PSS-rich solution. On the other hand, at a fixed PSS concentration (0.1 g/L), higher BSA concentrations than 0.3 g/L favor the formation of heterogeneous dendrites. While lower BSA concentrations (<0.3 g/L) will result into pure calcite crystals because of complete consumption of BSA molecules and surplus PSS left in the final stage. The formation of aragonite phase seems to have close relationship with surplus BSA in the final stage. But deep mechanism of controlling over polymorphs still needs further investigation.

Early Amorphous Mineral Precursor
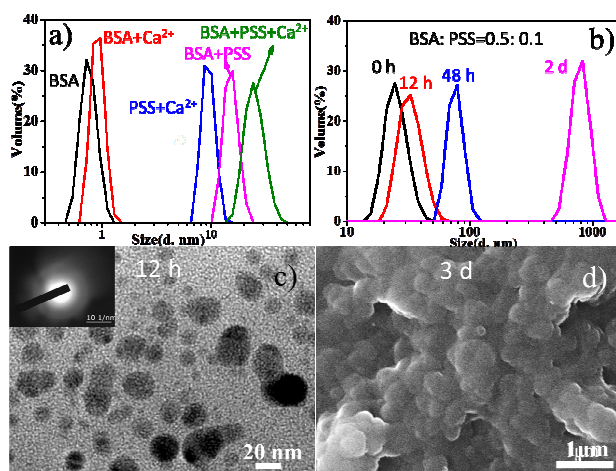
Fig. 3 (a) Particle size distribution of various additives or complexes before mineralization. (b-d) Size and morphology changes of mineral precursor in the gas diffusion procedure at different reaction time.

In our experiments, both BSA and PSS were applied in the gas diffusion procedure. The former is a globular protein[25] comprised of 582 amino acid residues (Fig. S5a, ESI†). [26] It has three secondary structures in aqueous solution, including α-, β- helix chain and random coil structure influenced by temperature, pressure, surfactant, and solvent. [27] Generally, its backbone has positive electricity surface below to the isoelectric point (4.6), and can serve as an effective soluble carrier protein for both anion and cation. The dynamic light scattering (DLS) measurement of BSA or BSA/CaCl$_2$ solution before mineralization shows the presence of 1 nm clusters. For a single BSA molecule, one will expect a diameter of the same order of magnitude. Meanwhile, a negatively charged polyelectrolyte of PSS is also applied, which bears a great deal of sulfonate groups (Fig. S5b, ESI†). [28] In the PSS/CaCl$_2$ solution,

DLS pattern shows aggregations with 10 nm in diameter, which have recently been proved to be the Ca-PSS globules[29] as PSS can bind to calcium ions.

In the Ca^{2+}/BSA+PSS solution, DLS analysis shows that the sizes become larger (~20 nm) than the individual component (Fig. 3a). The early organic additives may self-assemble into structured aggregations (denoted as BSA/PSS), stabilized by strong hydrogen bonds or electrostatic attraction between BSA and PSS molecules. These assemblies may provide nanospaces for the diffusion of calcium and carbonate ions, and induce the formation of irregular structures resembling a "solidified" dense liquid precursor phase (Fig. 3c). ED pattern proves these nascent particles are amorphous NPs (inset in Fig. 3c). Low contrast variation inside of the nanoparticles (NPs) indicates their liquid-like state. [30] The soft-condensed phase with a moderate degree fluidity and mobility enables them to aggregate together and even merge like droplets coalescing. The formation of the amorphous or liquid mineral precursor is usually the first step of non-classical crystallization. [31] Meanwhile, the increasing sizes with time proceeds mean that the mineral precursor will continuously aggregate or fuse together (Fig. 3b). After 2 days, the mineral precursor will deposit on the substrate, forming thin mineral films composed of droplet-like particles (Fig. 3d). XRD pattern confirms that the early mineral precursor is still in an amorphous phase (Fig. S7, ESI†).
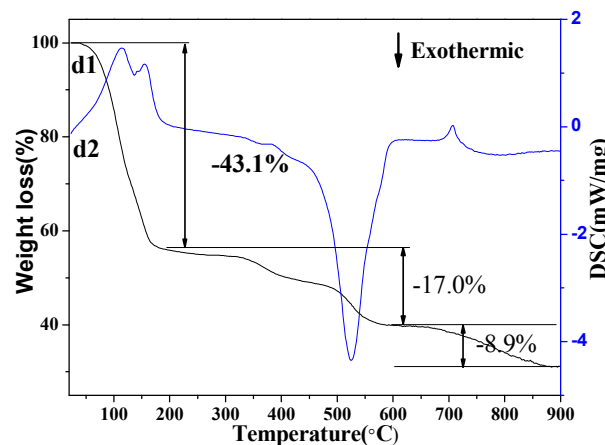

Fig. 4 TG (d1) and DSC (d2) curves of mineral films after 3 d.

The composition of this precursor is further investigated by TG-DSC analysis (Fig. 4). Thermogravimetry reveals three main stages of weight loss. The first stage is complete up to 190°C and involves a weight loss of 43.1%. This corresponds to two endothermic peaks in DSC curve due to the dehydration of the surface-bound and incorporated structural water. [32] The former water is lost at temperatures below 150°C, while the later is disappeared at 130-190°C. It can be calculated from integrated endothermic peak areas in DSC pattern that there are 21.8 wt% surface-bound water and 12.3 wt% structural water in the mineral precursor. The DSC curve shows an exothermic peak at 190-580°C, which is contributable to the degradation of organic additives. The third stage of weight loss is the characteristic decomposition of CaCO$_3$ (20.2 wt%) at above 650°C. Therefore, the molar ratio of structural water and calcium carbonate is up to 3.3, which implies that the mineral precursor is highly hydrated. [33] The early amorphous intermediate may be much like liquid amorphous calcium carbonate (LACC) [34] or polymer-induced liquid–precursor (PILP) phase. [35]

**Kinetic Measurements of CaCO$_3$ Nucleation**
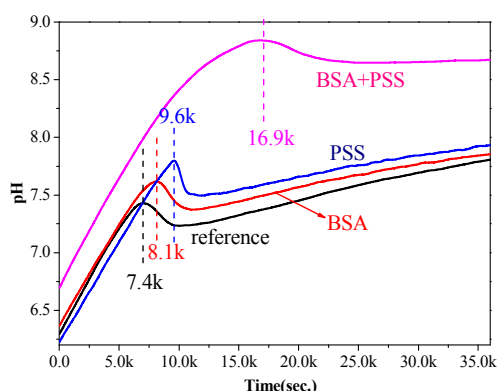
Fig. 5 pH-Time curves according to Kitano method with the different additives.

To better understanding the effects of different additives on the $CaCO_3$ nucleation, kinetic measurements of pHs versus time were carried out according to Kitano method (Experimental section, ESI†)[36]. In the pure $Ca(HCO_3)_2$ solution, pH/time curve (Fig. 5a) presents an upward tendency in a straight line at the beginning due to the constant release of CO_2 from the solution. A sharp pH drop means the $CaCO_3$ nucleation (pH = 7.4), and flattened increasing is caused by the subsequent transformation or crystallization of ACC. As many of other morphology controlling proteins,[37] BAS molecules show little inhibition effect on the nucleation process of $CaCO_3$ in the saturated $Ca(HCO_3)_2$ solution with BSA (Fig. 5b). Meanwhile, in the saturated $Ca(HCO_3)_2$/PSS solution, crystallization process doesn't change much compared with the reference case. Previous research shows that PSS is not active in the early stages of $CaCO_3$ mineralization, and its activity relies on the already preformed crystal nucleus.[38]

However, the $CaCO_3$ nucleation is inhibited greatly ($16.9*10^3$ s and pH = 8.7) when PSS and BSA are both introduced into the $Ca(HCO_3)_2$ saturated solution (Fig. 5d). This indicates that two additives are not simply mixed together. Given the observation from DLS analysis (Fig. 3b), it can be concluded that PSS and BSA molecules self-assemble into structured aggregations of BSA/PSS, which provide nanospace for diffusion of calcium and carbonate ions and lowere the solute concentration at the same time. The introduction of synergistic additives into the mineral solution allows the mineralization to undergo a nonclassical pathway, which is markedly influenced by the pre-organized assemblies in the mineral process.

Time-dependent experiments
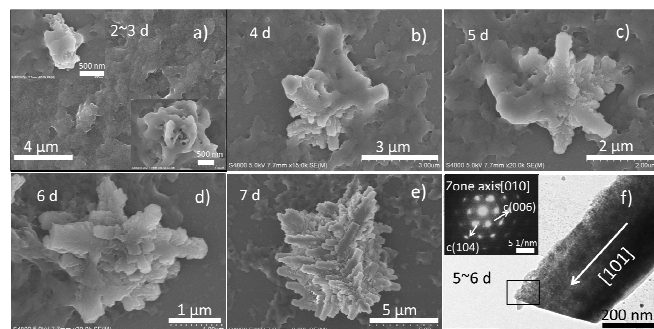
Fig. 6 SEM images (a-e) of time-dependent experiments, TEM and SAED analysis (f) of the local structure, growth orientation: [101].

Time-dependent experiments were performed to illustrate the formation and morphology evolution of dendrites. After 2-3 day,

scraggly mineral films will form as early mineral precursor on the substrate (Fig. 3d and Fig. 6a). Polarized optical microscopy (POM) image shows that they are still amorphous (Fig. S8a, ESI†). Later formed amorphous particles will stick to the raised points of the substrate, forming tapered or follower-like structures with smooth surface (insets in Fig. 6a). XRD pattern and FT-IR spectrum confirm that they are still in the amorphous phase (Fig. 7).

POM images show that crystallized domains occur on the mineral films after 4 days (Fig. S8b, ESI†). SEM image revealed that fibrous nanostructures are developed from the substrate (Fig. 6b). The gelatinous tips indicate that amorphous mineral precursor aggregates and coalesces at the growing points. During the growth of fibrous trunks, crystallized surfaces become coarse and particulate. Then small branches are seen to overgrow along the fibers (Fig. 6c-d). They will grow into multilayered dendrites soon (Fig. 6d-e). Time-dependent XRD and FT-IR studies prove that the early formed dendrites are calcite crystals (Fig. 7). It is noted that the some intermediates may grow faster into dendrites than others, which was determined by specific microenvironments.

But how are these dendrites formed in the mineral solution? We further detect the viscosity of early mineral solution, and find that it is rather viscous (Tab. S2, ESI†), which may arise from the organic additives and early formed amorphous mineral precursor. In such a solution circumstance, the diffusion of calcium and carbonate ions are is expected to decrease markedly. According to Oaki's reports,[39] the gel-like solution will lead to the instability of growing surface. In the present research, the original growth of main trunks is markedly retarded, but the formation of lateral branches is activated. The morphological change of dendrite-shaped superstructures can also be well explained by the property of the mineral solution. Evidences show that high polymer concentration and low temperature lead to higher solution viscosity. In such situation, leave-like (Fig. 1a) or dense branching (Fig. 1c) morphology was synthesized in a more viscous solution, where diffusion and convection of solute was effectively suppressed.

During the continuous growth of dendrites, mineral films were dissolved gradually and almost disappeared finally (Fig. 6e). Analysis of samples obtained after 5-6 days shows that they are calcite crystals (Fig. 7a and 7b). SAED pattern (inset in Fig. 5f) taken from the dendrite branch shows a typical calcite diffraction pattern with minor distortions, and it grows along [101] direction. TEM image show the well-defined facets at the tip ascribe to neutral {104} family (Fig. 6f).
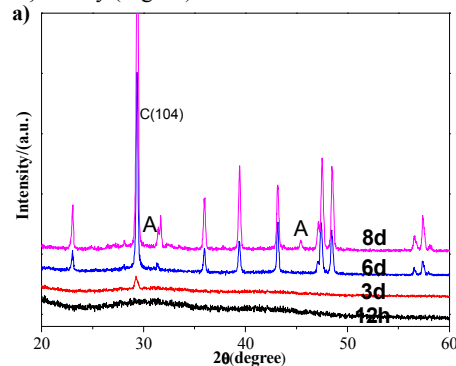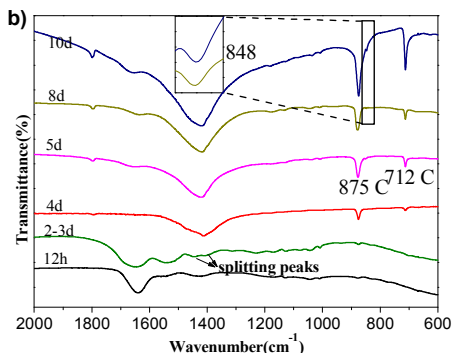
Fig. 7 (a) XRD pattern of samples at different times; (b) FTIR spectra of samples obtained at different time.

After a week or more, XRD and FT-IR spectra reveal that a tiny amount of aragonite crystals are present in the final products, which is according with the HRTEM analysis (Fig. 2). SEM images illustrate that the dendrite surfaces become gelatinous and smooth before the occurrence of aragonite phase (Fig. S9, ESI†). Aragonite shells may be developed from these amorphous coatings. If the coatings are not present on the external side of calcite scaffolding, mixtures of calcite and aragonite crystals will be produced rather than heterogeneous superstructures. But what are the major factors that induce the formation of amorphous mineral precursor and subsequent polymorph switch? To illustrate these questions, we further performed experiments to measure the solution variables during the mineralization.

Time-resolved measurement of solution variables
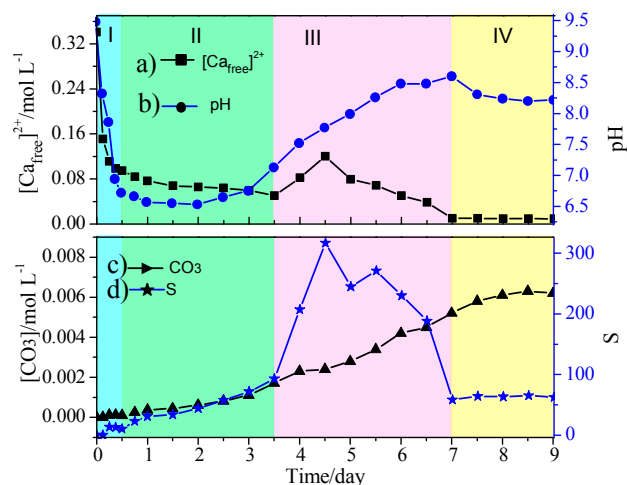
Fig. 8 Time-resolved profile of solute concentrations, pH values and supersaturation (S). The shaded areas mark the different stages of precipitation.

In parallel to the previous time-dependent experiments, we recorded the time-solved solution variables of pH values, free calcium ions and carbonate concentrations, which together yielded the underlying supersaturation profiles. Initially, concentration of free calcium ions (0.34 M) is far below the added calcium chloride (1 M) (Fig. 8a). Calcium ISE analysis confirms that there is no binding affinity between calcium ions and BSA molecules (Tab. S2, ESI†).[40] And the binding between PSS and calcium ions is much less, which is in accord with previous report.[38] Obviously, low concentration of free calcium ions is caused by the formation of PSS/BSA aggregations. Additionally, HPLC data show that initial PSS concentrations are also lower (0.037g/L), which further proves that the existences of self-assemblies in the mineral solution (Fig. S12b, ESI†).

The typical graphs show that the first stage of less than 12 h ascribes to the induction period. In this process, NH_3 and CO_2 continuously diffuse into the mineral solution, which, in turn, increases the pH values and carbonate ion concentrations. No $CaCO_3$ precipitation is detected because of low supersaturation. In the second stage, amorphous mineral precursors, such as mineral films and few embryonic dendrites (Fig. 6a), are observed on the substrate. The mineral solution is at neutral pHs (6.5-7.5), and there is more HCO_3^- ions as compared to CO_3^{2-} ions. Following the onset of nucleation (S>20), the calcium ion profile shows a slow drop due to its consumption during $CaCO_3$ precipitation. Wolf et al. demonstrated that a liquid-phase of $CaCO_3$ precursor droplets formed in supersaturated conditions at low pH value of 6.3,[41] which was quite similar to current solution condition. Bewernitz et al. claimed that liquid condensed phase formed in a bicarbonate-rich solution.[42] Recent reports also corroborated that a prenucleation cluster of $CaCO_3$ occurred at pHs ranging from 9.0 to 10.0 and prior to the formation of a metastable solid nucleus of ACC.[43] Given the present case, the pathway of metastable liquid phase may be preferred as has been proposed.

In the stage III, the solution pH value increase slowly to 8.3. The higher supersaturation (100-300) indicates that a great deal of ACC continuous to produce in this stage. SEM images manifest that dendrites are developed rapidly on the substrate, accompanying the dissolution of amorphous mineral films. During the dissolution process, calcium ions and BSA molecules may be released into the solution (Fig. S12a, ESI†).

Finally, the calcium ions and saturation of mineral solution decreased to relatively low levels (S=60-70). Additives of PSS and BSA were both at very low concentrations (Fig. S12, ESI†). In such situation, growth of aragonite phase on the calcite scaffolding was favorable as nucleation rate lowered to a low rate. The most probable scenario is that new aragonite particles nucleated on the existing additive-stabilized ACC, or on crystalline frameworks at later stages of the reaction, which was energetically favored over homogeneous nucleation. It was demonstrated that aragonite in general could not homogeneously nucleate under standard conditions.[44] Briefly, calcite crystals are easily synthesized at high solute concentrations and supersaturation levels, while aragonite phase forms under conditions of relatively low bulk component concentrations and supersaturation levels.

Conclusions

In summary, we demonstrated novel heterostructured dendrites with multilayered branches of calcite and aragonite controlled by the synergistic effects of bovine serum albumin and poly (sodium 4-styrenesulfonate). They were composed of the calcite scaffolding, the aragonite shell, and the amorphous calcium carbonate coatings. Morphology and polymorph switching of superstructure crystals are regulated availably by the reaction temperature, concentrations and ratios of the additives. The results further prove that the non-classical crystallization process is feasible and effective for the synthesis of calcium carbonate superstructure.

Acknowledgments

Notes and references

Anhui Province Key Laboratory of Metallurgical Emission Reduction &

Resources Recycling, Anhui University of Technology, Maanshan, Anhui, China. Email: thesea@ustc.edu.cn

1 K. Lee, W. Wagermaier, A. Masic, K. P. Kommareddy, M. Bennet, I. Manjubala, S. W. Lee, S. B. Park3, H. Cölfen and P. Fratzl, *Nat. Commun*, 2012, **3**, 725; b) V. C. Sundar, A. D. Yablon, J. L. Grazul, M. Ilan and J. Aizenberg, *Nature*, 2003, **424**, 899.

2 a) J. Jiang, M. R. Gao, Y. H. Qiu and S. H. Yu, *Nanoscale*, 2010, **2**, 2358; b) S. Kababya, A. Gal, K. Kahil, S. Weiner, L. Addadi, and A. Schmidt, *J. Am. Chem. Soc.*, 2015, **137**, 990; c) A. Gal, S. Weiner, and L. Addadi, *J. Am. Chem. Soc.*, 2010, **132**, 13208.

3 F. C. Meldrum, H. Cölfen, *Chem. Rev.*, 2008, **108**, 4332; b) N. Sommerdijk, G. de With, *Chem. Rev.*, 2008, **108**, 4499.

4 C. A. Orme, A. Noy, A. Wierzbicki, M. T. McBride, M. Grantham, H. H. Teng, P. M. Dove and J. J. DeYoreo, *Nature*, 2001, **411**,775.

5 J. H. Zhu, J. M. Song, S. H. Yu, W. Q. Zhang and J. X. Shi, *CrystEngComm*, 2009, **11**, 539.

6 J. H. Zhu, S. H. Yu, A. W. Xu and H. Cölfen, *Chem. Commun.*, 2009, **9** 1106.

7 E. G. Bellomo, T. J. Deming, *J. Am. Chem. Soc.*, 2006, **128**, 2276.

8 a) Y. Y. Kim, E. P. Douglas, L. B. Gower, *Langmuir*, 2007, **23**, 4862; b) S. Tugulu, M. Harms, M. Fricke, D. Volkmer, H. A. Klok, *Angew. Chem. Int. Ed.*, 2006, **45**, 7458.

9 H. Y. Li, L. A. Estroff, *Adv. Mater.*, 2009, **21**, 470; b) H. Y. Li, L. A. Estroff, *J. Am. Chem. Soc.*, 2007, **129**, 5480.

10 a)S. Kumar, T. Ito, Y. Yanagihara, Y. Oaki, T. Nishimura, T. Kato, *CrystEngComm*, 2010, **12**, 2021; b) X. Long, Y. R. Ma, K. R. Cho, D. S. Li, J. J. De Yoreo and L. M. Qi, *Cryst. Growth & Des.*, 2013,**13**, 3856

11 S. H. Yu, H. Cölfen, K. Tauer and M. Antonietti, *Nat. Mater.*, 2005, **4**, 51.

12 E. G. Bellomo and T. J. Deming, *J. Am. Chem. Soc.*, 2006, **128**, 2276.

13 a) A. W. Xu, M. Antonietti, S. H. Yu, H. Cölfen, *Adv. Mater.*, 2008, **20**, 1333; b) R. Q. Song, A. W. Xu, M. Antonietti, H. Cölfen, *Angew. Chem. Int. Ed.*, 2009, **48**, 395.

14 S. S.Wang, A. Picker, H. Cölfen and A. W. Xu, *Angew. Chem. Int. Ed.*, 2013, **52**,6317.

15 a) A. S. Aricò, P. Bruce, B. Scrosati, J. M. Tarascon and W. V. Schalkwijk, *Nat. Mater.*, 2005, **4**, 366; b) C. Liu, F. Li, L. P. Ma and H. M. Cheng, *Adv. Mater.*, 2010, **22**, 28.

16 a) A. V. Avizienis, C. Martin-Olmos, H. O. Sillin, M. Aono, J. K. Gimzewski and A. Z. Stieg, *Cryst. Growth & Des.*, 2013, **13**, 465; b) J. S. Huang, X. Y. Han, D. W. Wang, D. Liu and T. Y. You, *Appl. Mater. Interfaces*, 2013, **5**, 9148.

17 J. M. Ma, W. Guo, X. C. Duan, T. H. Wang, W. J. Zheng and L. Chang, *RSC Adv.*, 2012, **2**, 5944.

18 J. Y. Zheng, Z. L. Quan, G. Song, C. W. Kim, H. G. Cha, T. W. Kim, W. Shin, K. J. Lee, M. H. Jung and Y. S. Kang, *J. Mater. Chem.*, 2012, **22**, 12296.

19 H. Jia, X. T. Bai and L. Q. Zheng, *CrystEngComm*, 2011, **13**, 7252.

20 S. M. Porter. *Science*, 2007, **316**, 1302.

21 N. Nassif, N. Pinna, N. Gehrke, M. Antonietti, C. Jäger and H. Cölfen, *PNAS*, 2005, **102**, 12653.

22 N. Nassif, N. Gehrke, N. Pinna, N. Shirshova, K. Tauer, M. Antonietti and H. Cölfen, *Angew. Chem. Int. Ed.*, 2005, **44**, 6004.

23 L. S. Gomez-Villalba, P. López-Arce, M. Alvarez de Buergo and R. Fort, *Cryst. Growth& Des.*, 2012, **12**, 4844.

24 J. Zhu, L. Huang, M. Cui and L. Ma, *CrystEngComm*, 2015, **15**, 1010.

25 G. Jutz and A. Boker, *J. Mater. Chem.*, 2010, **20**, 4299.

26 K. Takeda, A. Wada, K. Yamamoto, Y. Moriyama and K. Aoki, *J. Protein Chem.*, 1989, **8**, 653.

27 a) M. Zhang, Y. Q. Dang, T. Y. Liu, H. W. Li, Y. Q. Wu, K. Wang and B. Zhu, *J. Phys. Chem. C*, 2013, **117**, 639; b) T. Chakraborty, I. Chakraborty, S. P. Moulik and S. Ghosh, *Langmuir*, 2009, **25**, 3062.

28 T. X. Wang, M. Antonietti and H. Cöfen, *Chem. Eur. J.*, 2006, **12**, 5722.

29 P. J. M. Smeets, K. R. Cho, R. G. E. Kempen, N. A. J. M. Sommerdijk and J. J. De Yoreo, *Nat. Mater.*, 2015, DOI: 10.1038/NMAT4193.

30 S. E. Wolf, L.Müller, R. Barrea, C. J. Kampf, J. Leiterer, U. Panne, T. Hoffmann, F. Emmerling and W. Tremel, *Nanoscale*, 2011, **3**, 1158.

31 H. Cölfen, Mesocrystals and Nonclassical Crystallization, Wily, Chichester 2008.

32 a) M. P. Schmidt, A. J. Ilott, B. L.Phillips, R. J. Reeder, Crys. Growth & Des., 2014, **14** , 938; b) J. Ihli, W. C. Wong, E. H. Noel, Y. Y. Kim, A. N. Kulak, H. K. Christenson, M. J. Duer and F. C. Meldrum, *Nat. Commun.*, 2014, **5**, 3169.

33 a)A. W. Xu, Q. Yu, W. F. Dong, M. Antonietti and H. Cölfen, *Adv. Mater.*, 2005, **17**, 2217; b) F. M. Michel, J. MacDonald, J. Feng, B. L.Phillips, L. Ehm, C. Tarabrella, J. B. Parise, R. J. Reeder, *Chem. Mater.*, 2008, **20**, 4720.

34 A. F. Wallace, L. O. Hedges, A. Fernandez-Martinez, P. Raiteri, J. D. Gale, G. A. Waychunas, S. Whitelam, J. F. Banfield and J. J. De Yoreo, *Science*, 2013, **341**, 885.

35 a) L. B. Gower and D. J. Odom, *J. Cryst. Growth*, 2000, **210**, 719; b) S. Wohlrab, H. Cölfen and M. Antonietti, *Angew. Chem. Int. Ed.*, 2005, **44**, 4087.

36 Y. Kitano, K. Park and D. W. Hood, *J. Geophys. Res.*, 1963, **67**, 4873.

37 J. Aizenberg, G. Lambert, S. Weiner and L. Addadi, *J. Am. Chem. Soc.*, 2002, **124**, 32.

38 A. Verch, D. Gebauer,M. Antonietti, H. Cölfen, *Phys. Chem. Chem. Phys.*, 2011, **13**, 16811.

39 Y. Oaki and H. Imai, *Cryst. Growth & Des.*, 2003, **3**, 711.

40 H. L. Zhai, W. Q Jiang, J. H. Tao, S. Y. Lin, X. B. Chu, X. R. Xu, R. K. Tang, *Adv. Mater.*, 2010, **22**, 3729.

41 S. E. Wolf, L. Mueller, R. Barrea, C. J. Kampf, J. Leiterer, U. Panne, T. Hoffmann, F. Emmerling and W. Tremel, *Nanoscale*, 2011, **3**, 1158.

42 M. A. Bewernitz, D. Gebauer, J. Long, H. Cölfen and L. B. Gower, *Faraday Discussions,* 2012, **159**, 291

43 D. Gebauer and H. Cölfen, *Nano Today*, 2012, **6**, 564.

44 a) A. W. Xu, W. F. Dong, M. Antonietti and H. Cölfen, *Adv. Funct. Mater.*, 2008, **18**, 1307; b) A. Kotachi, T. Miura and H. Imai, *Cryst. Growth & Des.*, 2004, **4**, 725.